Ocean Engineering 325 (2025) 120773

Contents lists available at ScienceDirect

Ocean Engineering

journal homepage: www.elsevier.com/locate/oceaneng

Research paper

A hybrid error correction method based on EEMD and ConvLSTM for offshore wind power forecasting

Lokmene Melalkia [a,**], Farid Berrezzek [a], Khaled khelil [a], Abdelhakim Saim [b,*], Radouane Nebili [a]

[a] Department of Electrical Engineering, Faculty of Science and Technology, Laboratory of Electrical Engineering and Renewable Energy (LEER), University of Souk Ahras, 41000, Algeria

[b] Nantes Université, Institut de Recherche en Energie Electrique de Nantes Atlantique, IREENA, UR 4642, Saint-Nazaire, F-44600, France

ARTICLE INFO

Keywords:
Offshore wind power
Forecasting
Renewable energy
Artificial intelligence

ABSTRACT

Efficient offshore wind power generation and seamless grid integration rely on accurate forecasting. However, the nonlinear and highly complex nature of ocean environmental conditions presents significant challenges, particularly for offshore applications. Thus, this paper introduces a novel hybrid deep learning model to address these challenges. The model employs Long Short-Term Memory (LSTM) to generate an initial offshore wind power forecast. The error signal is then extracted by subtracting the forecasted values from the actual wind power values. To capture nonlinear patterns in the forecasting error, the Ensemble Empirical Mode Decomposition (EEMD) decomposes the error signal into Intrinsic Mode Functions (IMFs) and a residual component. These components are forecasted using the Convolutional Long Short-Term Memory (ConvLSTM) model, which extracts spatial and temporal dependencies. The forecasted error components are summed to reconstruct the wind power error, which is subsequently added to the initial forecast to produce the adjusted wind power forecast. The model's performance is evaluated using an hourly wind power dataset from a Siemens SWT-3.6-120 Offshore turbine at the Amrumbank West wind farm. Comparative analysis with benchmark and hybrid models demonstrates superior accuracy, particularly for extended forecasting horizons of 2, 3, and 4 h. These findings underscore the proposed model's effectiveness in enhancing short-term offshore wind power forecasting.

1. Introduction

1.1. Background and motivation

The extending global demand for clean energy has placed wind power at the lead of renewable energy solutions. As an essential part of reducing carbon emissions and boosting sustainable energy, offshore wind power is more and more integrated into electrical grids worldwide (Cai et al., 2019). However, the nonlinear and highly unstable nature of wind creates substantial challenges to grid stability and efficient power generation. Thus, accurate offshore wind power forecasting plays an important role in mitigating these challenges, ensuring optimal energy integration as well as transmission, and improving the power system reliability (Guo et al., 2024).

1.2. Related works

The rising interest in offshore wind energy forecasting has led to the development of diverse models, each designed according to specific conditions and variables that determine their nature and functionality. These models can be categorized as presented in Fig. 1 by time horizon very short-term (minutes to hours), short-term (hours to days), medium-term (days to weeks), and long-term (weeks to years) (Khelil et al., 2021). Also, during the last few decades, several forecasting methods have been developed including physical, statistical, artificial intelligence (AI) (Mo et al., 2024), and hybrid approaches. Physical models, which depend on Numerical Weather Prediction (NWP), use factors like topography, temperature, humidity, and pressure for weather predictions but are limited by high computational demands and large

* Corresponding author. Nantes Université, Institut de Recherche en Energie Electrique de Nantes Atlantique, IREENA, UR 4642, Saint-Nazaire F-44600, France.
** Corresponding author. Department of Electrical Engineering, Faculty of Science and Technology, Laboratory of Electrical Engineering and Renewable Energy (LEER), University of Souk Ahras, Algeria.
E-mail addresses: l.melalkia@univ-soukahras.dz (L. Melalkia), f.berrezzek@univ-soukahras.dz (F. Berrezzek), khaled.khelil@univ-soukahras.dz (Khaled khelil), abdelhakim.saim@univ-nantes.fr (A. Saim), ra.nebili@univ-soukahras.dz (R. Nebili).

https://doi.org/10.1016/j.oceaneng.2025.120773
Received 19 December 2024; Received in revised form 10 February 2025; Accepted 21 February 2025
Available online 3 March 2025

dataset requirements, making them less suitable for small-scale forecasting (Zhang et al., 2022a).

Statistical approaches, such as ARMA (Erdem et al., 2014) and ARIMA (Shukur and Lee, 2015), are simpler and more effective for short-term forecasting by analysing historical time series data. However, they struggle with nonlinear and nonstationary data and are less effective for long-term forecasts (Guo et al., 2024).

With advances in soft computing, AI methods have become popular for handling nonlinear problems in wind power forecasting (Guo et al., 2023). These include techniques like extreme learning machine (ELM) (Sun and Wang, 2023) (Yang et al., 2024), support vector machine (SVM) (Yu et al., 2018), artificial neural networks (ANN) (Shukur and Lee, 2015), convolutional neural networks (CNN) (Bouadjila et al., 2024) (Garg and Krishnamurthi, 2023), long short-term memory (LSTM) (Moharm et al., 2020), and gated recurrent units (GRU) (Zhao et al., 2023). However, despite the progress in the AI model's performance, they encounter challenges due to their susceptibility to uncertainties and variations in wind speed characteristics across different sites (Guo et al., 2024). To boost further the precision of forecasting results, researchers have begun to explore hybrid methods that integrate multiple approaches to enhance their robustness, adaptability, and forecasting accuracy. This shift toward hybrid models represents a significant advancement in the field, as it leverages the strengths of different techniques to address the complexities of time series forecasting tasks (Wang et al., 2024). For example, in (Zhao et al., 2023), the authors combined CNN and LSTM to improve short-term power load forecasting, while in (Shukur and Lee, 2015), a hybrid Kalman Filter-ANN model based on ARIMA was proposed for forecasting wind speed. In (Garg and Krishnamurthi, 2023), Sherry et al. introduce a hybrid model that merges the autoencoder technique with a CNN as the encoder and LSTM as the decoder.

The forecasting method is closely tied to the characteristics of the input data and forecasting wind power remains challenging due to inherent uncertainties. To address this, various studies have introduced pre-processing techniques, such as signal decomposition (Berrezzek et al., 2019). For example (Zhang et al., 2022a), proposes a combined model using Discrete Wavelet Transform (DWT), Seasonal Autoregressive Integrated Moving Average (SARIMA), and LSTM to predict short-term offshore wind power. To simplify input data and facilitate model training, particularly with non-stationary and nonlinear data (Berrezzek et al., 2019), proposed a hybrid forecasting model that uses Empirical Mode Decomposition (EMD) and combines the LSTM network with ARIMA. Wind speed datasets from Inner Mongolia, China, were decomposed using EMD to reduce the complexity data, LSTM to predict high-frequency sub-sequences with high entropy, and ARIMA to predict low-frequency sub-sequences with one residual. Although EMD still faces challenges with mode mixing (Wan et al., 2023), an improved form, EEMD was utilized in a hybrid wind speed prediction model proposed by the authors in (Hou et al., 2024). This model combines SARIMA, EEMD, and LSTM, with EEMD employed to decompose the nonlinear residual series into intrinsic mode functions (IMFs) and sub-residual sequences. Each IMF and sub-residual sequence is then independently fitted to an LSTM model, and the predicted results are combined with linear periodic and trend sequences to produce the final wind speed prediction. This approach leverages the effectiveness of EEMD decomposition in enhancing prediction accuracy. EEMD decomposition has also been shown to enhance model performance in several studies (Xin et al., 2024) (Zhang et al., 2022b) (Shahid et al., 2023). However, despite the strong performance of these models, further improvements are limited, as efforts have largely concentrated on refining model architecture rather than addressing errors generated by the model itself.

To further enhance model accuracy, several studies have focused on identifying sources of error and applying error correction methods to adjust forecasting errors. In (Moharm et al., 2020), for instance, the difference between predicted and actual wind power values is computed, and an ARIMA model is applied to predict these error values, thereby refining the original forecast accordingly. In (Jiang and Liu, 2023), the authors employ particle swarm optimization and error correction mechanisms using LSTM to enhance wind power forecasting. In (Wilkerson and Wilkerson, 2008), the authors utilize an ensemble model for initial wind power forecasting and apply an error correction method based on Bidirectional LSTM to capture temporal correlations in wind power sequences. Yet the extreme fluctuations in wind power forecasting errors still present challenges that impact the adjustment of the original forecast.

1.3. Objectives and contributions

To address the limitations of existing wind power forecasting models, which primarily focus on model enhancement without adequately addressing forecasting errors, a new error-correction approach is proposed. This method combines the LSTM model for the initial forecast with an error correction technique that utilizes Ensemble Empirical Mode Decomposition (EEMD) to handle the fluctuating and highly random nature of wind power forecasting errors by capturing nonlinear

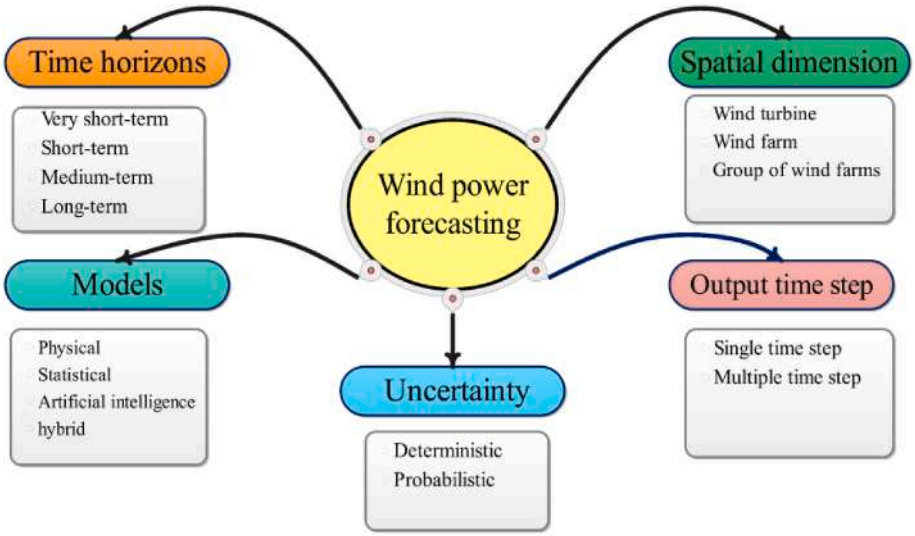

Fig. 1. Classification of wind power forecasting.

patterns and reducing noise. Additionally, ConvLSTM is employed to capture spatial and temporal dependencies within the forecasting error signal. The key contributions of this work are as follows.

1. A hybrid deep learning forecasting model, based on a novel error correction framework, is proposed for short-term offshore wind power forecasting. This model provides a solution for adapting and refining the original forecast.
2. EEMD decomposition is used to preprocess the offshore wind power forecasting error signal, effectively capturing its nonlinearity and reducing noise, which enhances the accuracy of error forecasting.
3. Integration of the ConvLSTM model enables to capture of both spatial and temporal dependencies within the error sequences, further enhancing forecast precision and reliability.

The rest of the paper is organized as follows: Section 2 details the structure of the proposed forecasting model and the methods used in this study. Section 3 covers the materials, implementation, and experimental setup of the predicting model. The experimental results along with a comparative analysis are presented in Section 4. Finally, Section 5 provides the concluding remarks.

2. Methodology

2.1. The structure of the proposed model

The main steps of the proposed LSTM error correction-based forecasting scheme (LSTM-EEMD-ConvLSTM), as illustrated in Figs. 2 and 3, are outlined as follows.

1. The meteorological features, along with the original wind power, are provided as inputs to the LSTM model to generate the forecasted wind power $\widehat{P}_n$.
2. The forecasted wind power values $\widehat{P}_n$ are then subtracted from the actual wind power values P_n to obtain the wind power forecasting error Er_n.
3. EEMD decomposition is applied to decompose the error Er_n into IMFs $(IMF_1, \ldots\ldots, IMF_{15})$ and a residual component Res.
4. The decomposed IMFs and residual component are fed into the ConvLSTM block, which forecasts each component $(\widehat{Imf_1}, \widehat{Imf_2} \ldots\ldots \widehat{Imf_l}$ and $\widehat{Res})$ where $l = 1, \ldots, 15$. These forecasted components are then summed to reconstruct the original forecasted error $\widehat{Er_n}$.
5. Finally, the initial wind power forecast from the LSTM model, $\widehat{P}_I[n]$, is combined with the predicted error from the error correction model, $\widehat{Er_n}$, to produce the final wind power forecast, $\widehat{P}_f[n]$.

2.2. Long short-term memory LSTM

LSTM is a type of recurrent neural network (RNN) that provides effective solutions in handling nonlinear problems such as time series forecasting due to its capability of handling long-term dependencies in sequence data (Wan et al., 2023). The key idea behind LSTMs is to use a set of memory cells that can maintain information over a longer period. These memory cells are connected to three gates: an input gate, an output gate, and a forget gate. The complete LSTM structure is illustrated in Fig. 4.

The input gate i_t controls how much new information is allowed into the memory cell C_t (Hou et al., 2024). Using equation (1) it takes the current input X_t and the previous output H_{t-1} as inputs, and then passes these through a sigmoid function σ to obtain a value between 0 and 1 (Xin et al., 2024). This value is then multiplied by a candidate vector u_t, which represents the new information to be added to the memory cell, and also the updated cell state C_t.

$$i_t = \sigma(W_{xi}X_t + W_{hi}H_{t-1} + W_{ci} \odot C_{t-1} + b_i) \tag{1}$$

where σ is the sigmoid activation function which is defined as in equation (2).

$$\sigma(X) = \frac{1}{1 - e^{-x}} \tag{2}$$

The forget gate f_t controls how much information should be

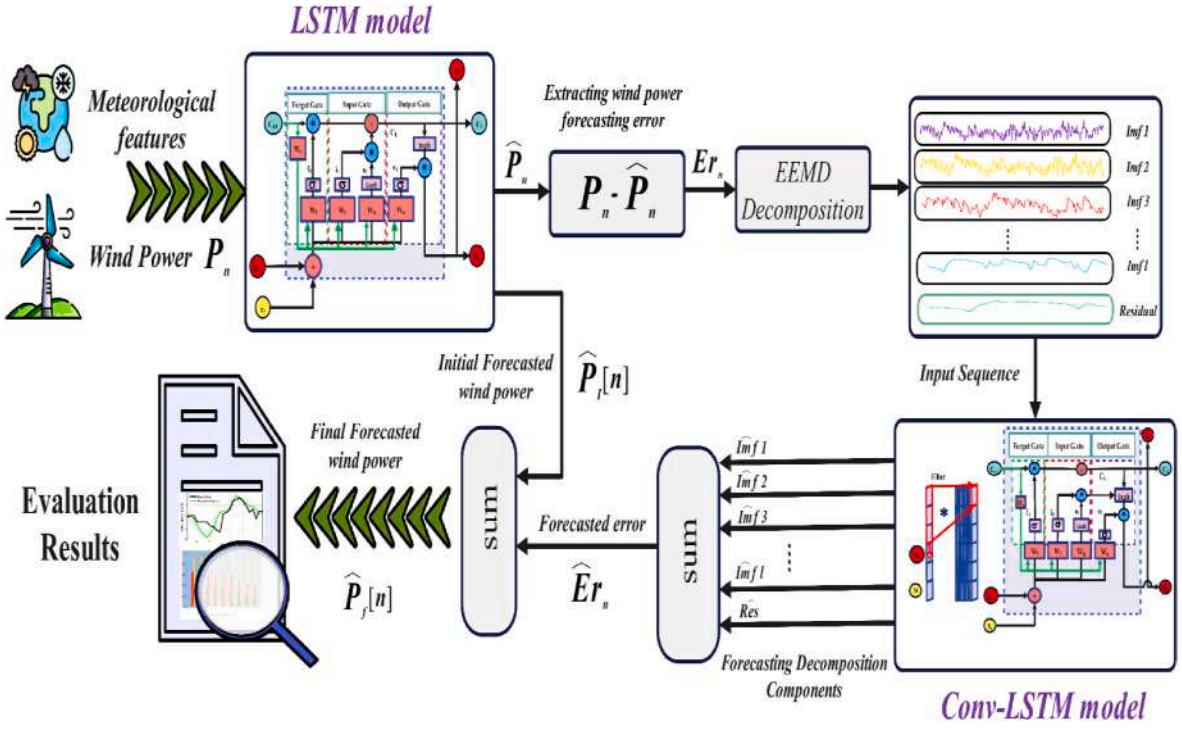

Fig. 2. The proposed LSTM-Error Correction (EEMD-ConvLSTM) forecasting structure.

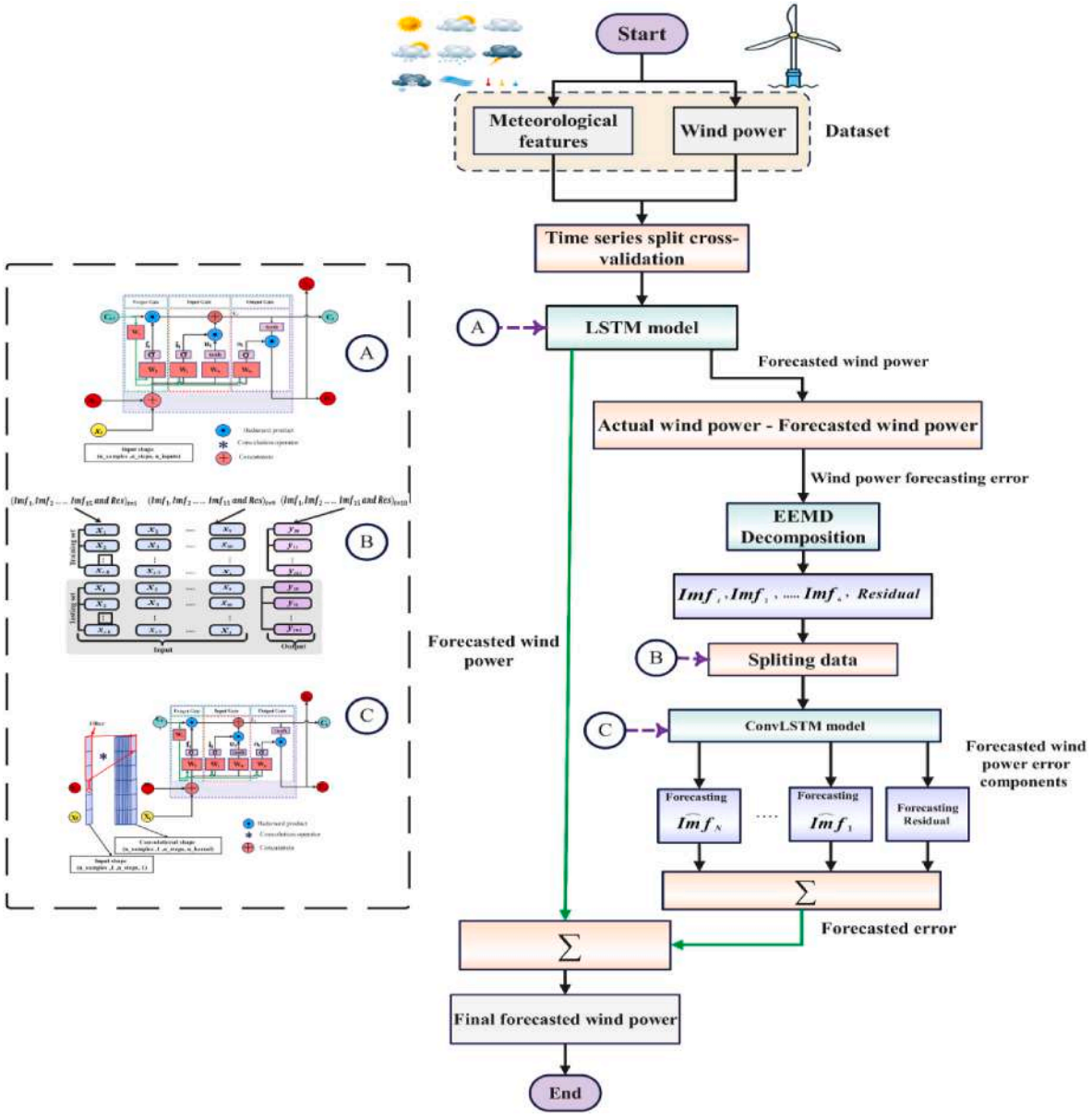

Fig. 3. Flowchart of the proposed forecasting scheme.

discarded from the memory cell. As in equation (3), it takes the current input and the previous output as inputs and then passes these through a sigmoid function to obtain a value between 0 and 1. This value is then multiplied by the current state of the memory cell to determine how much information should be forgotten.

$$f_t = \sigma\left(W_{xf}X_t + W_{hf}H_{t-1} + W_{cf} \odot C_{t-1} + b_f\right) \tag{3}$$

the candidate vector u_t represents potential new information to be added to the memory cell state by using equation (4), generated as part of the internal update mechanism.

$$u_t = \tanh(W_{xu}X_t + W_{hu}H_{t-1} + b_u) \tag{4}$$

Where tanh is the hyperbolic tangent function defined in equation (5) (Zhang et al., 2022a).

$$\tanh(X) = \frac{e^x - e^{-x}}{e^x + e^{-x}} \tag{5}$$

The memory cell state C_t is updated by combining the candidate vector u_t with the previous cell state C_{t-1}, modulated by the input and forget gates equation (6).

$$C_t = f_t \odot C_{t-1} + i_t \odot u_t \tag{6}$$

The output gate O_t controls how much information is allowed to leave the memory cell and contribute to the final output using equation (7) (Zhang et al., 2022b). The value of O_t is multiplied by the current state of the memory cell, which is also passed through a tanh function to normalize the output equation (8).

$$O_t = \sigma(w_{xo}X_t + W_{ho}H_{t-1} + W_{co} \odot C_{t-1} + b_0) \tag{7}$$

$$h_t = O_t \odot \tanh(C_t) \tag{8}$$

The three gates in an LSTM enable it to selectively store, forget, and retrieve information over time by controlling the flow of information through the memory cell (Zhao et al., 2023).

2.3. Convolutional LSTM network

ConvLSTM network is an extension of LSTM with convolutional

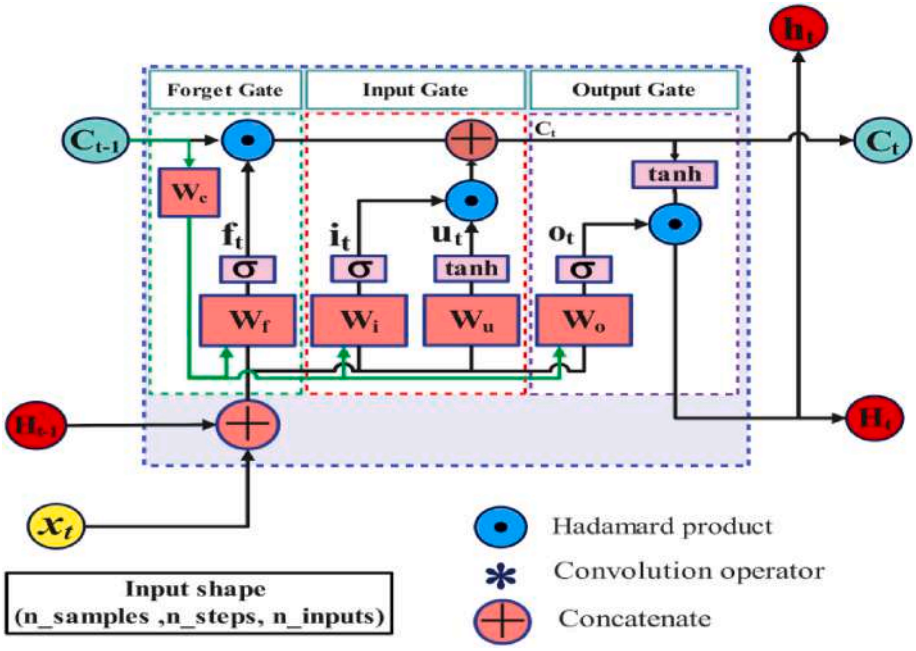

Fig. 4. LSTM structure.

structures in both the input-to-state and state-to-state transitions. The primary issue with traditional LSTM is that it does not use any spatial information in the connections between input and state, or between state and state transitions. ConvLSTM incorporates convolutional operations into the LSTM structure, allowing it to learn spatial-temporal patterns in the input (Shahid et al., 2023). In the ConvLSTM the inputs are changed with convolution operations, which consists of several filters to extract important features and flow through the LSTM cells as 3D input instead of being just a 1D vector with features. The structure of ConvLSTM is shown in Fig. 5 and is mathematically described by equation 9 through 14 (Shahid et al., 2023).

$$i_t = \sigma(W_{xi} * X_t + W_{hi} * H_{t-1} + W_{ci} \odot C_{t-1} + b_i) \quad (9)$$

$$f_t = \sigma(W_{xf} * X_t + W_{hf} * H_{t-1} + W_{cf} \odot C_{t-1} + b_f) \quad (10)$$

$$C_t = f_t \odot C_{t-1} + i_t \odot u_t \quad (11)$$

$$u_t = \tanh(W_{xu} * X_t + W_{hu} * H_{t-1} + b_u) \quad (12)$$

$$O_t = \sigma(w_{xo} * X_t + W_{ho} * H_{t-1} + W_{co} \odot C_{t-1} + b_0) \quad (13)$$

$$h_t = O_t \odot \tanh(C_t) \quad (14)$$

2.4. Ensemble Empirical Mode Decomposition (EEMD)

Empirical Mode Decomposition (EMD) is a signal processing method

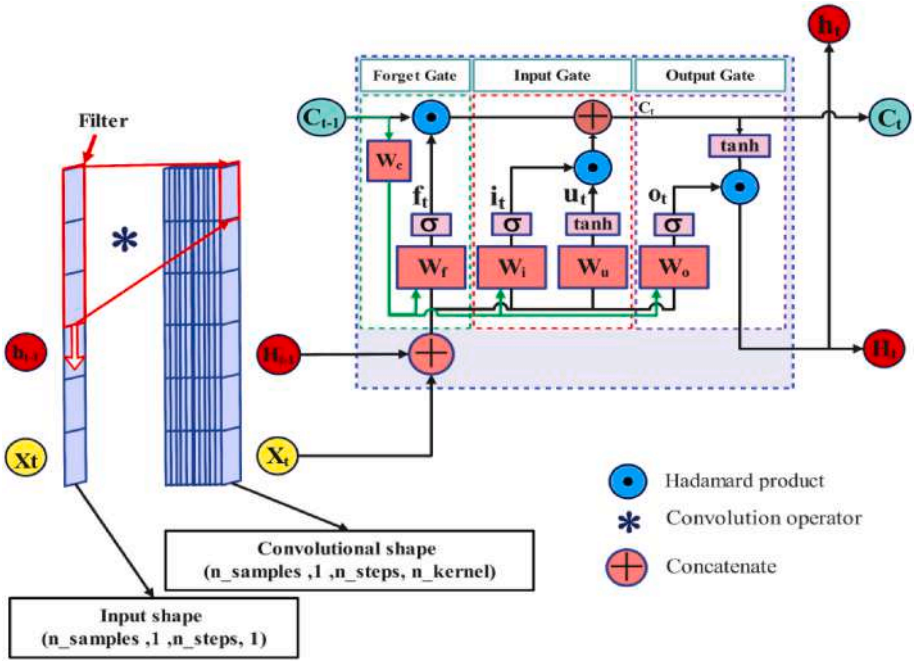

Fig. 5. ConvLSTM structure.

for analysing non-stationary and nonlinear signals by decomposing them into Intrinsic Mode Functions (IMFs). These IMFs represent distinct oscillatory modes corresponding to various frequency scales of the original signal and are derived through the Hilbert-Huang transformation (Berrezzek et al., 2019). An IMF is defined by two criteria: the number of extrema (local maxima and minima) and zero crossings must either be equal or differ by no more than one. The second criterion is that the average value of the envelope created by the local maxima and the envelope generated by the local minima should be zero at any given position. Although EMD is useful for wind power forecasting, it has a notable limitation called mode mixing, which occurs when a single IMF contains signals with widely varying scales or when signals of similar scales are distributed across different IMF components (Greenland et al., 2016). This describes a case where an intrinsic mode function (IMF) contains components of varying frequencies, likely due to occasional signals and data interruptions. To address this issue, the advanced Ensemble Empirical Mode Decomposition (EEMD) technique was developed. EEMD enhances nonlinearity capture and noise reduction by introducing random Gaussian white noise to the signal, which helps mitigate mode mixing by distributing noise uniformly across all frequencies and scales (Hauber et al., 2016). As a result, this approach significantly improves the correlation between the derived intrinsic mode functions (IMFs) and the original raw series (Hauber et al., 2016). Fig. 6 presents a flowchart of the EEMD decomposition, achieved through the following steps.

Step 1, as outlined in equation (15), involves introducing the Gaussian white noise series $n^s(t)$ (s = 1,2, …,s+1), which are mutually distinct, to the wind power forecasting error V(t). This process generates a novel signal denoted as $V^s(t)$ (Jiang and Liu, 2023).

$$V^s(t) = V(t) + n^s(t) \tag{15}$$

In Step 2, the new signal, combined with white noise, is decomposed using EMD into multiple oscillatory modes, referred to as IMFs, along with a residual. The formulation of $V^s(t)$ is subsequently provided in equation (16).

$$V^s(t) = \sum_{m=1}^{M} IMF_m^{EMD,s}(t) + R_M^{EMD,s}(t)\ m = 1, 2, 3 \ldots\ldots M \tag{16}$$

The variables $IMF_m^{EMD,s}(t)$ and $R_M^{EMD,s}(t)$ refer to the IMF components

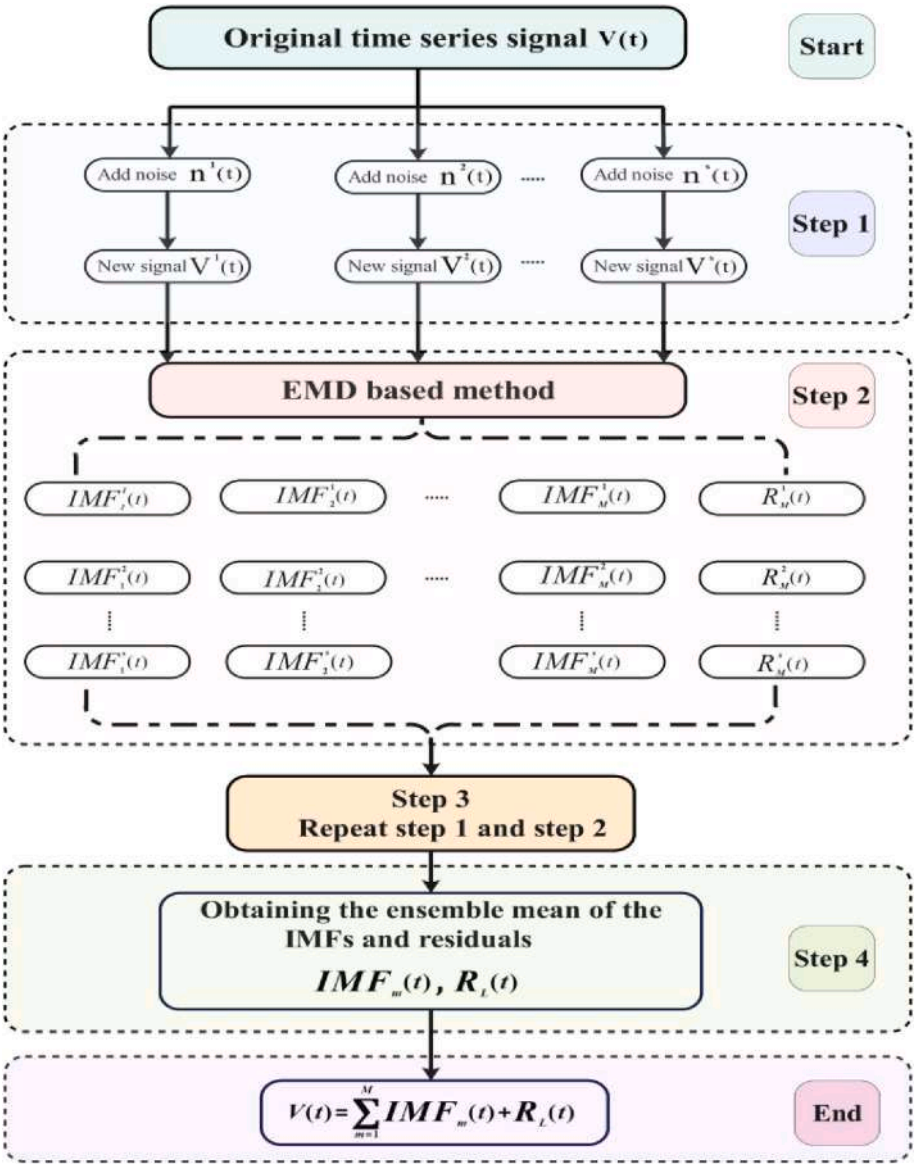

Fig. 6. EEMD Decomposition flowchart.

and residual sequence, respectively, which are obtained after the addition of white noise and EMD decomposition

Step 3 consists of repeating Steps 1 and 2 S times, introducing a distinct Gaussian white noise in each iteration (Zhang et al., 2022b).

$$\left(IMF_1^{EMD,s}(t), IMF_2^{EMD,s}(t), IMF_3^{EMD,s}(t)\ldots\ldots\ldots\ldots IMF_M^{EMD,s}(t), R_M^{EMD,s}(t)\right)$$
$$s=1,2,3\ldots\ldots N$$

Step 4 involves calculating the ensemble mean of the corresponding Intrinsic Mode Functions (IMFs) and residual components. The Gaussian white noise is eliminated by averaging the IMF values, as expressed in equations (17)–(19) (Xin et al., 2024).

$$IMF_m(t)=\frac{1}{N}\sum_{s=1}^{N} IMF_m^{EMD,S}(t)\ m=1,2,3\ldots\ldots M \tag{17}$$

$$R_L(t)=\frac{1}{N}\sum_{s=1}^{N} R_M^{EMD,s} \tag{18}$$

$$V(t)=\sum_{m=1}^{M} IMF_m(t)+R_L(t) \tag{19}$$

2.5. Error correction method

Due to the nonlinear, random, and fluctuating nature of wind power, which impacts the performance of forecasting models, this paper proposes an error correction model (EEMD-ConvLSTM) to refine the forecasting results generated by the initial model. Specifically, the LSTM network is utilized for its simplicity and efficiency, particularly in addressing sequence-to-sequence problems (Yu and Hutson, 2024). Initially, the LSTM model, following successful training, produces the first wind power forecast $\widehat{P}_n$. Subsequently, the wind power forecasting error is calculated, as illustrated in Fig. 7, by subtracting the forecasted value $\widehat{P}_n$ from the actual wind power value P_n, in accordance with equation (20) (Moharm et al., 2020).

$$Er_n=P_n-\widehat{P}_n \tag{20}$$

The Spearman correlation coefficient (ρ), as defined in equation (21), is utilized to evaluate the monotonic relationship between forecasting errors and wind power data, regardless of linearity [30]. A ρ value close to 1 signifies a strong positive monotonic relationship, while a value near −1 indicates a strong negative monotonic relationship, and 0 reflects no relationship. This analysis provides insights into the factors influencing forecasting accuracy [31].

$$\rho=1-\frac{6\sum_{i=1}^{n} d_i^2}{n(n^2-1)} \tag{21}$$

Where *di* represents the difference between the ranks of two variables (the forecasting error and wind power) for each observation while n represents the total number of observations. Using equation (21), a ρ value of 0.6792 is obtained, indicating a moderate positive correlation and emphasizing the connection between error components and wind power dynamics. This suggests that identifying and addressing these error patterns can substantially enhance forecasting accuracy [31]. The EEMD-ConvLSTM model is then utilized to forecast the wind power error, which is subsequently added to the initial LSTM wind power forecast to produce a corrected prediction. This approach addresses variations missed in the initial forecast, thereby reducing overall error and improving the accuracy of the final wind power output.

2.6. Performance evaluation metrics

Wind power forecasting is inherently uncertain, making perfect precision challenging to achieve. Consequently, accurate evaluation of forecasts is critical for assessing model performance. This study employs several metrics to evaluate forecasting accuracy: Root Mean Square

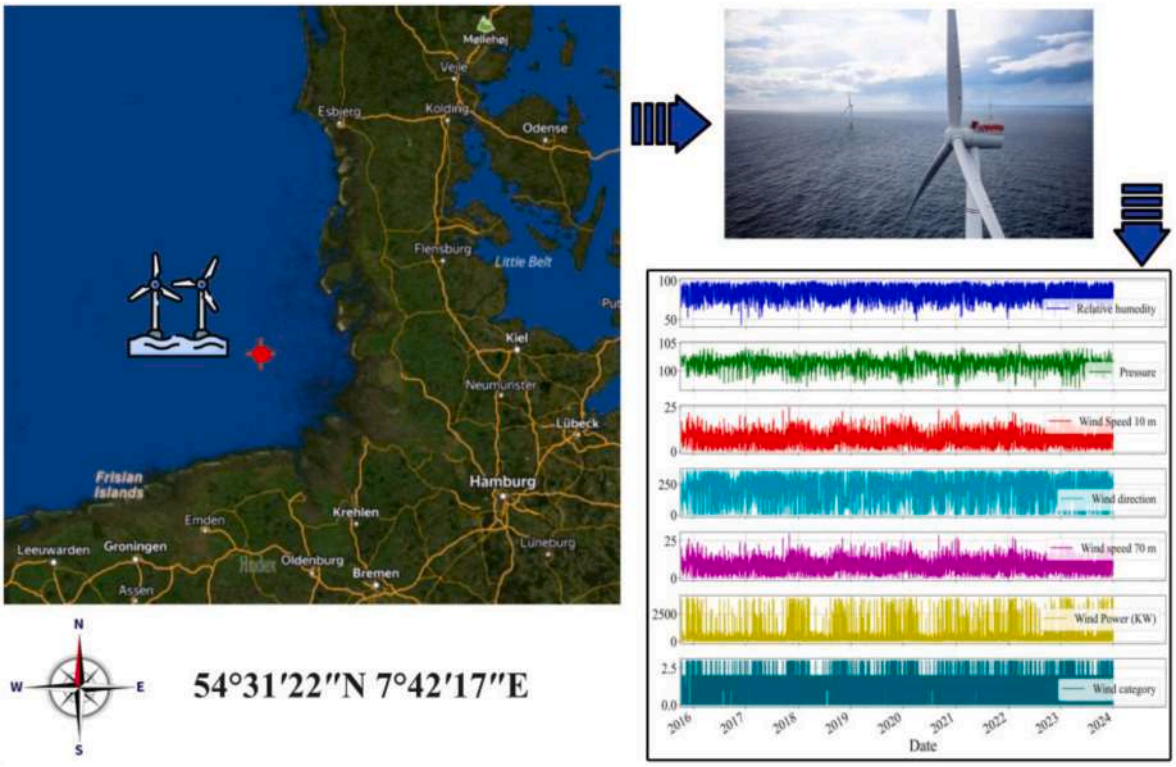

Fig. 7. Dataset turbine location.

Error (RMSE, equation (22)), which emphasizes larger errors; Mean Absolute Error (MAE, equation (23)), which measures the average error magnitude; Mean Absolute Percentage Error (MAPE, equation (24)); and the coefficient of determination (R^2, equation (25)), which reflects the proportion of variance in actual data explained by the model. Together, these metrics provide a comprehensive evaluation of the model effectiveness in forecasting wind power output, considering both precision and error magnitude (Zhao et al., 2024).

$$RMSE = \sqrt{\frac{1}{N}\sum_{t=1}^{N}(y_t - \hat{y}_t)^2} \tag{22}$$

$$MAE = \frac{1}{N}\sum_{t=1}^{N}(y_t - \hat{y}_t) \tag{23}$$

$$MAPE = \left(\frac{1}{N}\sum_{t=1}^{N}\frac{(y_t - \hat{y}_t)}{y_t}\right) \times 100 \tag{24}$$

$$R^2 = 1 - \frac{\sum_{t=1}^{N}(y_t - \hat{y}_t)^2}{\sum_{t=1}^{N}(y_t - \overline{y}_t)^2} \tag{25}$$

Where N is the number of data points. y_t and $\hat{y}_t$ represent the actual and the forecasted values respectively.

To ensure the robustness of the performance comparisons, statistical significance was assessed using p-values, calculated through paired t-tests between the proposed model and the other models using equation (26) (Wilkerson and Wilkerson, 2008). The paired *t*-test was chosen because it accounts for the dependency between the forecasting errors of different models when evaluated on the same dataset, ensuring a fair and reliable comparison. Additionally, applying equation (27) the 95% Confidence Intervals (CIs) were computed for MAE and RMSE using the standard error of the mean (Greenland et al., 2016). These intervals provide a range within which the true model performance is expected to lie, with a 95% level of confidence, offering insights into the precision and reliability of the error metrics. For R^2 and MAPE, point estimates were reported without confidence intervals, as these metrics are typically interpreted based on their absolute values rather than their variability.

$$t = \frac{\overline{d}}{S_d/\sqrt{N}} \tag{26}$$

$$CI = \overline{x} \pm t_{\alpha/2,N-1} \cdot \left(\frac{S}{\sqrt{N}}\right) \tag{27}$$

Where $\overline{d}$ is the mean of the differences between the paired errors of the two models and S_d is the standard deviation of the differences, while $\overline{x}$ is the sample mean of the metric $t_{\alpha/2,N-1}$ is the critical value from the t-distribution for a 95% confidence level, $N-1$ is the degrees of freedom and S is the sample standard deviation of the metric (Hauber et al., 2016).

3. The proposed hybrid forecasting scheme

3.1. Dataset

To assess the performance of the proposed forecasting scheme, a dataset from a Siemens SWT-3.6-120 Offshore wind turbine is employed. This turbine is situated at the Amrumbank West offshore wind farm in the North Sea, approximately 35 km northwest of Heligoland Island and 18 km southwest of the Amrumbank sandbank, with the exact location depicted in Fig. 7. Focusing on a single turbine allows the models to capture site-specific conditions and turbine-related factors.

The dataset, collected over 1-h intervals, contains meteorological features including wind speed (m/s) at 70 m, air pressure (P in Pascals), relative humidity (%), wind direction (°), wind speed (m/s) at 10 m, wind category (high, medium, low), and wind power (kW) for a single turbine, these six features selected were chosen based on their direct influence on wind power generation, relative humidity and air pressure impact the atmosphere state and, consequently, wind direction and speed at 70m, especially at turbine hub height, are essential components for Kinetic Energy while wind speed at 10m provides insights into local wind patterns, while wind category helps classify operational conditions for the turbines. Using more features may capture complex dynamics but risks overfitting and higher computational costs without significant accuracy gains. Fewer features could lose essential information, compromising predictions. The six chosen features balance accuracy, interpretability, and efficiency. Moreover, a larger dataset allows the model to generalize better across different conditions, ultimately improving forecasting accuracy, spanning from January 2015 to December 2023, the dataset includes 72,334 samples. A detailed statistical description is provided in Table 1. The Spearman's Rank Correlation Coefficient between wind speed and wind power is $\rho = 0.97$, indicating a strong relationship that facilitates power generation through accurate modelling using the Weibull distribution. This relationship is influenced by factors such as wind speed, blade pitch angle, and shaft speed, with the generated power described by equation (26).

$$P_m = \frac{1}{2}\rho v_w^3 \pi r^2 C_p \tag{26}$$

Where P_m is the power (W) extracted from the wind, ρ is the air density (kg/m^3), r is the rotor blade radius (m), v_w is the wind speed (m/s), and C_p is the performance coefficient.

3.2. Overview of the forecasting scheme

To ensure consistent model performance, data preprocessing steps were implemented. Min-max scaling normalization was applied to all input features. Wind power, being the target variable, and wind category, being a categorical variable, were not normalized. Due to the very small number of missing values, we employed Spline Interpolation to accurately fill in the gaps in the data. The dataset is split into 85% for model development and 15% for final testing to ensure a thorough evaluation of the proposed model. A time series split cross-validation with k = 12 is applied to the 85% portion, creating training and validation sets. This approach helps the LSTM model learn wind power patterns and temporal dependencies during training. The validation sets are then used to identify forecasting errors and train the error correction model (EEMD-ConvLSTM), allowing for accurate error modelling under varied conditions.

Choosing the right timestep is key to preparing inputs for the LSTM model. Shorter timesteps capture more detail but may limit the dataset available for feature extraction. On the other hand, longer timesteps simplify the data but risk missing important details and overfitting. Through trial and error, the optimal interval for training the models was found to be 9 timesteps. A timestep of 9, combined with six meteoro-

Table 1
Dataset statistical details.

	Count	Mean	Std	Min	Max
Relative humidity	72334	84.54	8.08	43.5	100
Air pressure	72334	101.38	1.09	96.9	104.83
Wind direction 70m	//	208.11	92.69	0	359.94
Wind speed 10m	//	7.67	3.54	0.3	24.8
Wind category	//	nan	nan	0	3
Wind speed 70 m	//	8.98	4.15	1.3	30.38
Wind power (kW)	//	532.64	807.7	0	3993.6

logical features and wind power dataset, is used to construct input matrices with dimensions 7 × 9 times as x_i (i = 1, …, 9), where each input represents 9 timesteps ($t-8, t-7, \ldots, t$), as depicted in Fig. 8. These inputs are then fed into the proposed model to forecast wind power 1 h ahead at t+1.

In general, choosing the hyperparameter of deep learning models manually is challenging and demands a substantial understanding of the problem at hand. In this study, the GridSearchCV tool is utilized for hyperparameter tuning (Zhao et al., 2024). Table 2 outlines the hyperparameters utilized for the LSTM model and the error correction model. Following successful training, the model is validated to extract wind power errors, as defined by equation (20).

As depicted in Fig. 9, the subtracted error exhibits notable nonlinearity, randomness, and significant fluctuations, highlighting the need to capture its complex nonlinear relationships to enhance error forecasting. To address this, EEMD decomposition is employed to break down the subtracted error into a series of Intrinsic Mode Functions (IMFs), each representing distinct frequency components. The residual component (Res), which cannot be further decomposed into additional IMFs, reflects the overall trend. Fig. 10 illustrates the EEMD decomposition of the wind power forecasting error, resulting in 15 levels (15 IMFs). Figs. 9 and 10 visually confirm the effectiveness of EEMD in denoising, depicting a clear reduction in high-frequency fluctuations in the error signal after decomposition where the Denoised Signal exhibits a smoother and less noisy behaviour compared to the Wind Power Error signal. To quantify this noise reduction, we calculated the Signal-to-Noise Ratio (SNR) by Equation (27) before and after applying EEMD to the wind power error signal (Zheng et al., 2024). The SNR increased from 8.14 dB to 13.36 dB after EEMD decomposition, representing a

Table 2
Forecasting models hyper-parameters.

Model	Hyperparameter	Value
LSTM	Forecasting timestep	9
	Number of input variables	7
	Optimizer	Adam
	Dropout	0.2
	Batch size	64
	Epochs	250
	Learning rate	0.001
	Number of LSTM layers	2
	Number of Neural Network layers	3
	activation function	ReLU
Conv-LSTM	Number of input variables	16
	forecasting timestep	9
	Epochs	300
	Optimizer	Adam
	Batch size	16
	Learning rate	0.001
	Number of ConvLSTM layers	3
	Number of Neural Network layers	2
	ConvLSTM Filters	(128,64,32)
	ConvLSTM Kernel size	(3,3)
	ConvLSTM Activation	ReLU

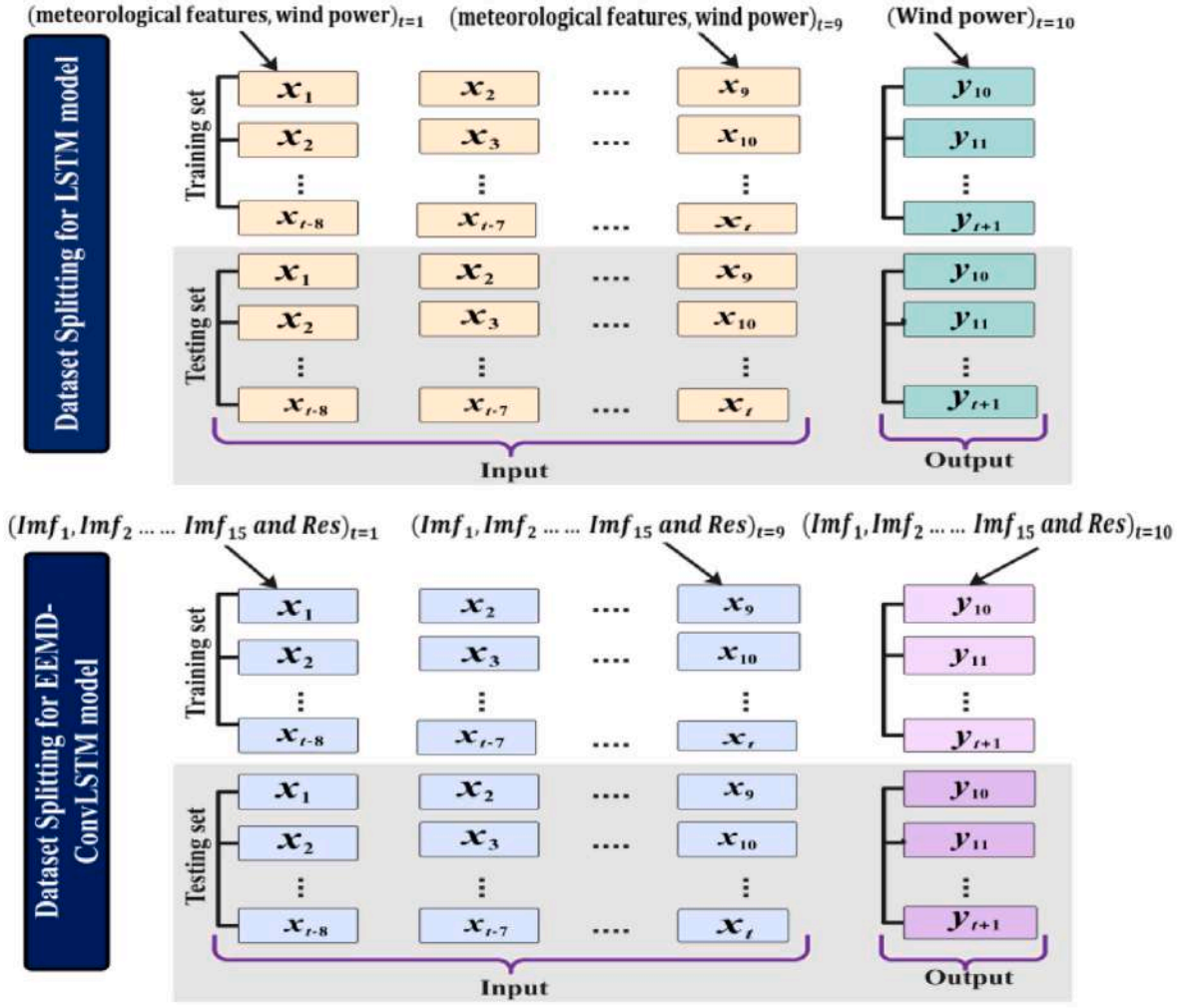

Fig. 8. Inputs splitting.

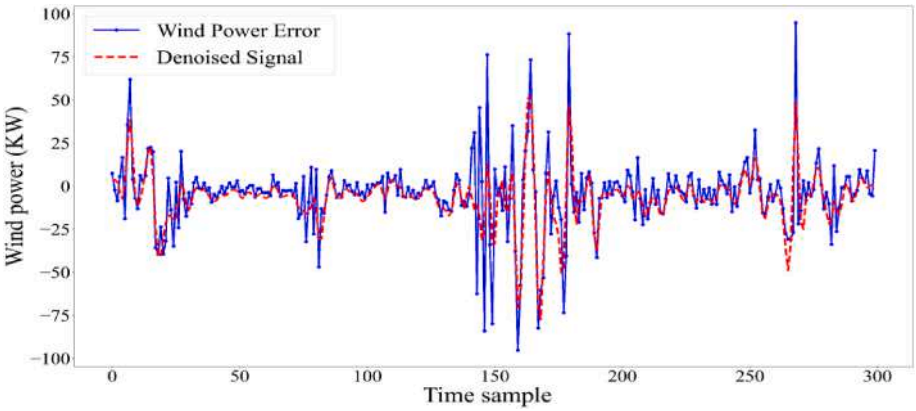

Fig. 9. Noise reduction in wind power forecasting error through EEMD decomposition.

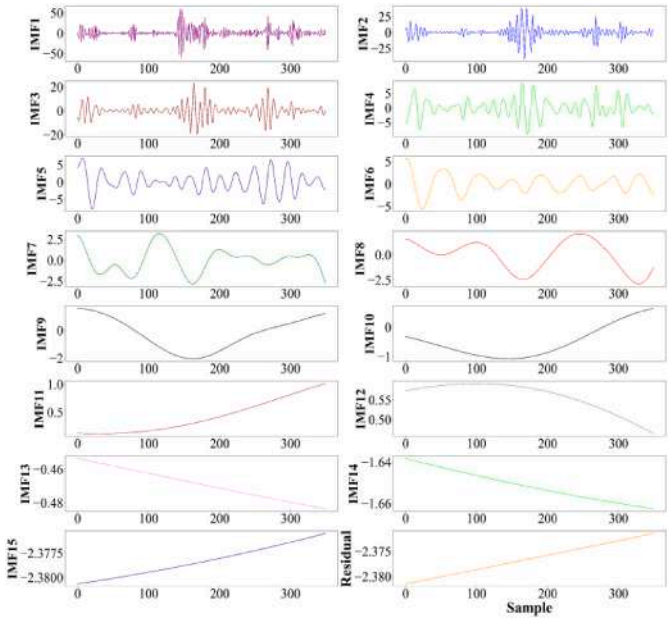

Fig. 10. EEMD decomposition for wind power error.

significant improvement of 64.13%. To ensure that EEMD preserves the important features of the original signal while denoising, we calculated the Pearson correlation coefficient between the original error signal and the reconstructed signal obtained after EEMD. The correlation coefficient reached a high value of 0.985, indicating a strong positive correlation. This statistically significant correlation implies that the reconstructed signal captures the essential trends and patterns of the original error signal, while effectively removing noise (Yu and Hutson, 2024).

$$SNR = 10\ log_{10}\frac{P_1}{P_2} \tag{27}$$

A timestep of 9 along with error decomposition components $(Imf_1, Imf_2 \ldots\ldots Imf_{15}\ and\ Res)$, is utilized to construct input matrices with dimensions (16 × 9): $x_i\ (i = 1, \ldots, 9)$ where each input represents 9 timesteps $(t-8, t-7, \ldots, t)$ as shown in Fig. 9. These inputs are then applied to the ConvLSTM model to forecast the error decomposition components. The forecasted IMFs and residuals $(\widehat{Imf}_1, \widehat{Imf}_2 \ldots\ldots \widehat{Imf}_{15}\ and\ \widehat{Res})$ are summed back together to reconstruct the 1-h ahead of forecasted error at the time $t+1$. The final step involves combining the forecasted wind power $\widehat{Er}_n$ from the LSTM model with the forecasted error $\widehat{Er}_n$ generated by the EEMD-ConvLSTM model to obtain the final forecasted wind power $\widehat{P}_f[n]$ as illustrated in Figs. 2 and 3.

4. Simulations results and discussion

To assess the effectiveness of the proposed model, a comprehensive comparative analysis was performed. Its performance was first benchmarked against several established forecasting models, including ConvLSTM, ARIMA, BP neural networks, basic LSTM, LSTM with error correction using ConvLSTM, and SVR. Additionally, a comparison was conducted against several hybrid models, including CNN-BiGRU, Autoencoder (AE-GRU), EEMD-LSTM, CNN-LSTM, and LSTM-ARIMA, to further substantiate its superiority. Finally, the model forecasting capabilities were evaluated across different time horizons to analyse its adaptability to various temporal scales.

4.1. Comparison with benchmark models

Table 3, Figs. 14 and 15 demonstrate that the LSTM Error-Correction (EEMD-ConvLSTM) model outperforms benchmark models in wind power forecasting, achieving the lowest MAE (4.22 ± 0.31), RMSE (9.31 ± 0.80), and MAPE (0.19%), along with the highest R^2 value of 0.9811. These results highlight the effectiveness of incorporating error correction techniques, particularly the combination of EEMD and ConvLSTM,

Table 3
Performance Comparison of the LSTM-Error Correction Model (EEMD-ConvLSTM) with Benchmark Models in the offshore wind power forecasting (kW).

Model	MAE (95% CI)	RMSE (95% CI)	R^2	MAPE	p-value vs. Proposed Model
LSTM Error-Correction (EEMD-ConvLSTM)	**4.22 ± 0.31**	**9.31 ± 0.80**	**0.9811**	**0.19**	-
LSTM Error-Correction (ConvLSTM)	4.60 ± 0.40	13.64 ± 1.20	0.9772	0.25	0.03
ConvLSTM	5.74 ± 0.56	18.33 ± 1.72	0.9496	0.36	0.02
LSTM	6.14 ± 0.64	22.69 ± 2.16	0.9355	0.53	0.015
BPNN	8.32 ± 0.82	31.90 ± 2.99	0.8937	0.83	<0.001
ARIMA	11.36 ± 1.45	39.62 ± 3.85	0.8619	1.12	<0.001
SVR	23.22 ± 2.20	48.61 ± 4.74	0.7835	1.58	<0.001

in improving forecasting accuracy. The EEMD-ConvLSTM approach excels at decomposing complex error signals into IMFs, allowing the ConvLSTM to process each component separately, thereby capturing both local and global patterns in the signal. The p-values in Fig. 11 for comparisons with other models 0.03 for LSTM Error-Correction (ConvLSTM), 0.02 for ConvLSTM, and <0.001 for BPNN, ARIMA, and SVR confirm that the performance improvements are statistically significant. The LSTM Error-Correction (ConvLSTM) model, which uses ConvLSTM for error correction without incorporating EEMD, also performs better due to the error correction techniques, with an MAE of 4.60 ± 0.40, RMSE of 13.64 ± 1.20, MAPE of 0.25%, and R^2 of 0.9772. However, its slightly higher error rates and lower R^2 value compared to the EEMD-ConvLSTM model underscore the added benefit of EEMD in handling the nonlinearity and non-stationarity of error signals which led to an 8.3% reduction in MAE (from 4.60 to 4.22) and a 31.7% reduction in RMSE (from 13.64 to 9.31), demonstrating its effectiveness in noise reduction and improving forecasting accuracy. The ConvLSTM model, which lacks error correction, achieves an MAE of 5.74 ± 0.56, RMSE of 18.33 ± 1.72, MAPE of 0.36%, and R^2 of 0.9496, outperforming the standard LSTM model (MAE: 6.14 ± 0.64, RMSE: 22.69 ± 2.16, MAPE: 0.53%, R^2: 0.9355). This represents a 6.5% reduction in MAE (from 6.14 to 5.74) and a 19.2% reduction in RMSE (from 22.69 to 18.33) demonstrating the importance of convolutional layers in capturing spatio-temporal dependencies, which are critical for forecasting. Traditional models, such as BPNN, ARIMA, and SVR, exhibit clear limitations, with BPNN achieving moderate performance (MAE: 8.32 ± 0.82, RMSE: 31.90 ± 2.99, MAPE: 0.83%, R^2: 0.8937) and ARIMA (MAE: 11.36 ± 1.45, RMSE: 39.62 ± 3.85, MAPE: 1.12%, R^2: 0.8619) and SVR (MAE: 23.22 ± 2.20, RMSE: 48.61 ± 4.74, MAPE: 1.58%, R^2: 0.7835) performing even less. These results emphasize the inability of traditional statistical and machine learning methods to manage the nonlinear complexities and high variability of wind power data, further underscoring the superiority of deep learning-based approaches, particularly those incorporating error correction techniques.

Fig. 12 presents the performance of various forecasting models compared to actual wind power values, with the top and bottom subplots offering close-up views of specific time intervals. These detailed views highlight the models ability to capture anomalies and variations in wind power. The LSTM-Error Correction (EEMD-ConvLSTM) model consistently aligns closely with actual values, showing its robustness in handling both smooth and abrupt changes. The LSTM-Error Correction (ConvLSTM) model also performs well, though with slightly greater deviations. In contrast, traditional models such as ARIMA, SVR, BPNN, and basic LSTM exhibit noticeable errors, particularly during rapid fluctuations, reflecting their limited capacity to handle the complex nature of wind power.

For a clearer and more focused comparison, Fig. 13 highlights the developed models, namely the LSTM Error-Correction (EEMD-ConvLSTM), LSTM Error-Correction (ConvLSTM), and ConvLSTM. By showing only these leading models, it becomes evident that the proposed approach stands out for its superior accuracy and reliability, consistently excelling in capturing both gradual and sudden variations in wind power.

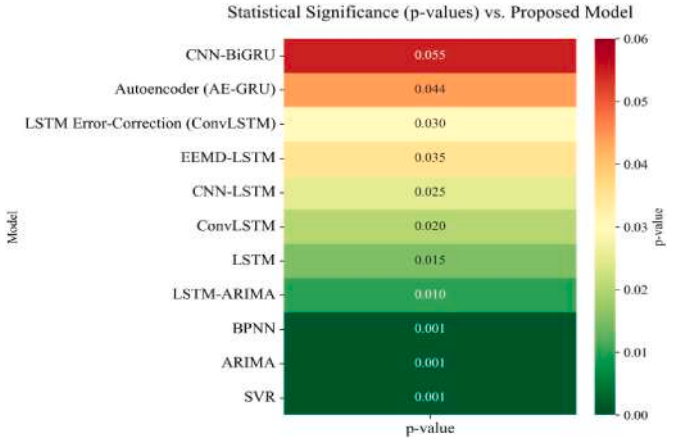

Fig. 11. The P-Value of Model Performance vs. Proposed Model.

4.2. Comparison with hybrid models

To further substantiate the superiority of the proposed model a comparison against several hybrid models has been conducted. Table 4 and both Figs. 14 and 15 highlight the performance of the hybrid models, which combine multiple architectures and techniques to enhance wind power forecasting accuracy further. The proposed model remains the best-performing model, with an MAE of 4.22 ± 0.31, RMSE of 9.31 ± 0.80, MAPE of 0.19%, and R^2 of 0.9811, confirming the effectiveness of integrating EEMD and ConvLSTM for error correction. The CNN-BiGRU model, which combines CNN to extract spatial features with Bidirectional GRU to capture temporal dependencies in both forward and backward directions, achieves competitive performance, with an MAE of 4.51 ± 0.38, RMSE of 10.75 ± 0.90, MAPE of 0.22%, and R^2 of 0.9768. However, the proposed model further enhances accuracy, reducing MAE by 6.4% and RMSE by 13.4%, demonstrating its performance compared to the CNN-BiGRU model. The Autoencoder (AE-GRU) model, which integrates an Autoencoder with GRU, also performs better, achieving an MAE of 4.77 ± 0.42, RMSE of 11.90 ± 0.98, MAPE of 0.26%, and R^2 of 0.9724. The autoencoder reduces the dimensionality of the input data, extracting essential features that are then processed by the GRU for temporal modelling. The EEMD-LSTM model, which combines EEMD with a standard LSTM, achieves an MAE of 5.12 ± 0.50, RMSE of 13.42 ± 1.18, MAPE of 0.30%, and R^2 of 0.9659, outperforming standalone LSTM but falling short of the EEMD-ConvLSTM model. The CNN-LSTM model, which integrates CNN with LSTM, achieves an MAE of 5.58 ± 0.54, RMSE of 15.84 ± 1.50, MAPE of 0.35%, and R^2 of 0.9553, demonstrating the benefits of combining spatial and temporal modelling. The LSTM-ARIMA model, which combines LSTM with ARIMA, achieves an MAE of 6.35 ± 0.60, RMSE of 19.75 ± 1.80, MAPE of 0.44%, and R^2 of 0.9401, highlighting the limitations of ARIMA in handling nonlinear patterns. The p-values in Fig. 11 for comparisons with the proposed model 0.055 for CNN-BiGRU, 0.044 for AE-GRU, and 0.01 for LSTM-ARIMA confirm that the performance differences are statistically significant. These results underscore the importance of hybrid models in wind power forecasting, as they effectively combine the strengths of multiple techniques to handle the complexity and variability of wind power data, paving the way for more accurate forecasts.

4.3. Forecasted error analysis

Fig. 16 illustrates a comparative analysis of the actual and forecasted errors generated by the EEMD-ConvLSTM model and the ConvLSTM model, compared against actual error values. This comparison helps us understand how well these models minimize and correct errors in the original wind power forecasting. All error series mark pronounced fluctuations, particularly around zero, indicative of the highly dynamic nature of wind power generation. The plot shows that the EEMD-ConvLSTM model generally maintains a lower magnitude of error compared to the ConvLSTM model. The upper peaks and lower peaks of the error values are less extreme, While the ConvLSTM model also follows the actual error closely, there are instances where the deviations are more pronounced compared to the EEMD-ConvLSTM model. The difference in performance between these two models calls to attention the added value of integrating the EEMD approach for error correction.

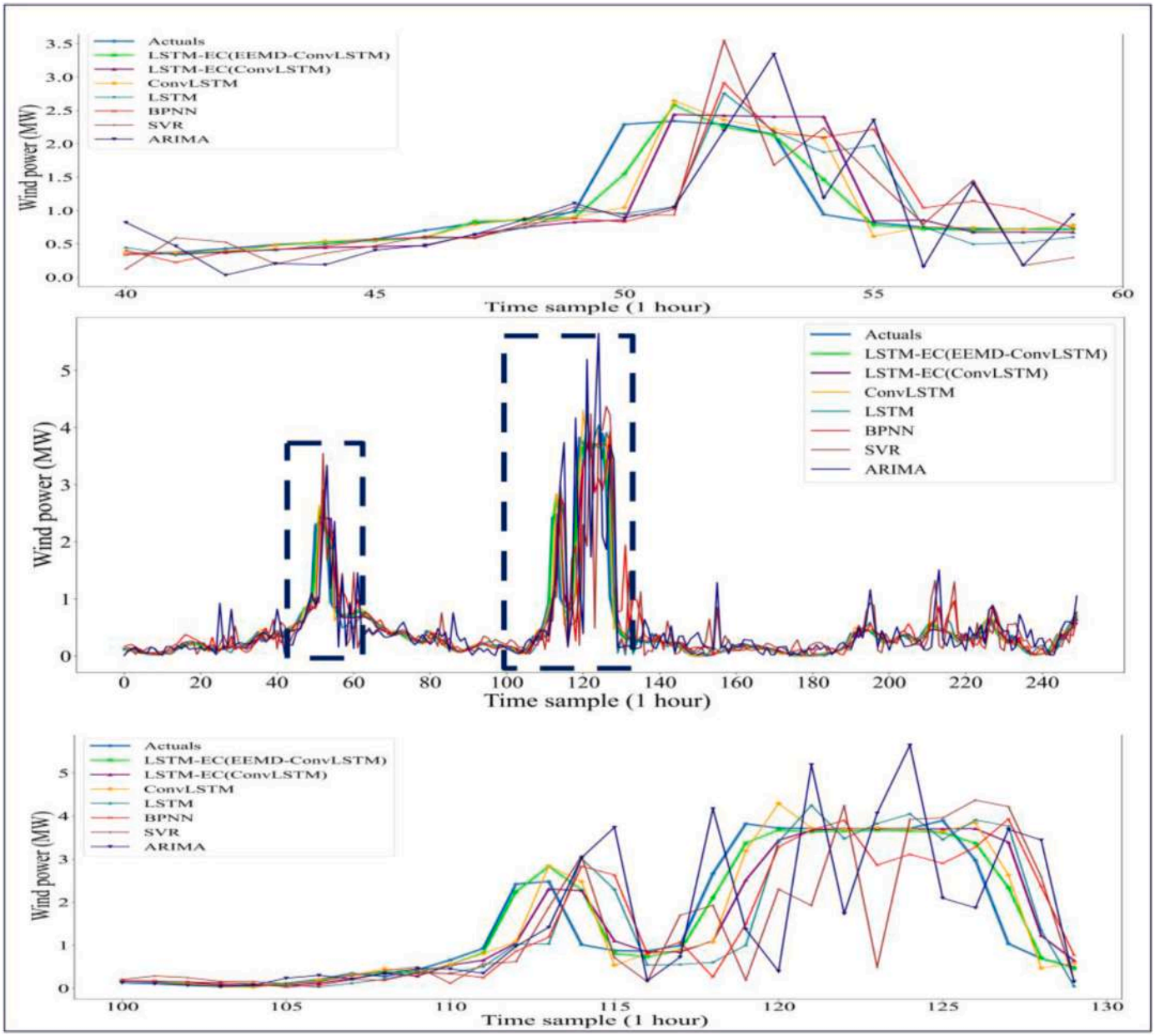

Fig. 12. Wind power forecasting compared to benchmark models.

4.4. *Different time step forecasting*

The forecasting results, summarized in Table 5 and illustrated in Fig. 17, evaluate the performance of various models in forecasting wind power across multiple forecasting horizons one-step, two-step, three-step, and four-step. The models evaluated include LSTM-Error Correction (EEMD-ConvLSTM), LSTM-Error Correction (ConvLSTM), ConvLSTM, LSTM, BPNN, ARIMA, and SVR. Among these, the proposed model consistently outperforms the other models.

The evaluation encompasses several models, including LSTM-Error Correction (EEMD-ConvLSTM), LSTM-Error Correction (ConvLSTM), ConvLSTM, LSTM, BPNN, ARIMA, and SVR. Among these, the proposed model consistently outperforms the other models.

4.4.1. *Two-step forecasting*

As the forecasting horizon extends to two steps ahead, all models experience a slight decline in performance due to the increased uncertainty of predicting further into the future. Nevertheless, as shown in Table 5 and Fig. 17, the proposed model maintains its superiority, achieving an MAE of 7.605 kW, RMSE of 13.66 kW, and R^2 of 0.9396. While there is a modest increase in errors compared to the one-step forecast, the model retains a high degree of accuracy, with a MAPE of just 0.39%. The LSTM-Error Correction (ConvLSTM) and ConvLSTM models also exhibit increased errors, with MAE values of 8.801 kW and 11.323 kW, respectively. In contrast, traditional models such as ARIMA and SVR show a significant decline in performance, highlighting their limitations in handling the increased non-linear complexities associated with longer forecasting horizons.

4.4.2. *Three-steps forecasting*

The three-step forecasting results from Table 5 and Fig. 17 demonstrate that the proposed model continues to deliver acceptable performance, although its accuracy begins to decline as the forecasting horizon extends. The model achieves an MAE of 12.252 kW, RMSE of 26.703 kW, and R^2 of 0.8936. While these errors are higher compared to the one-step and two-step forecasts, the model maintains a relatively low error rate

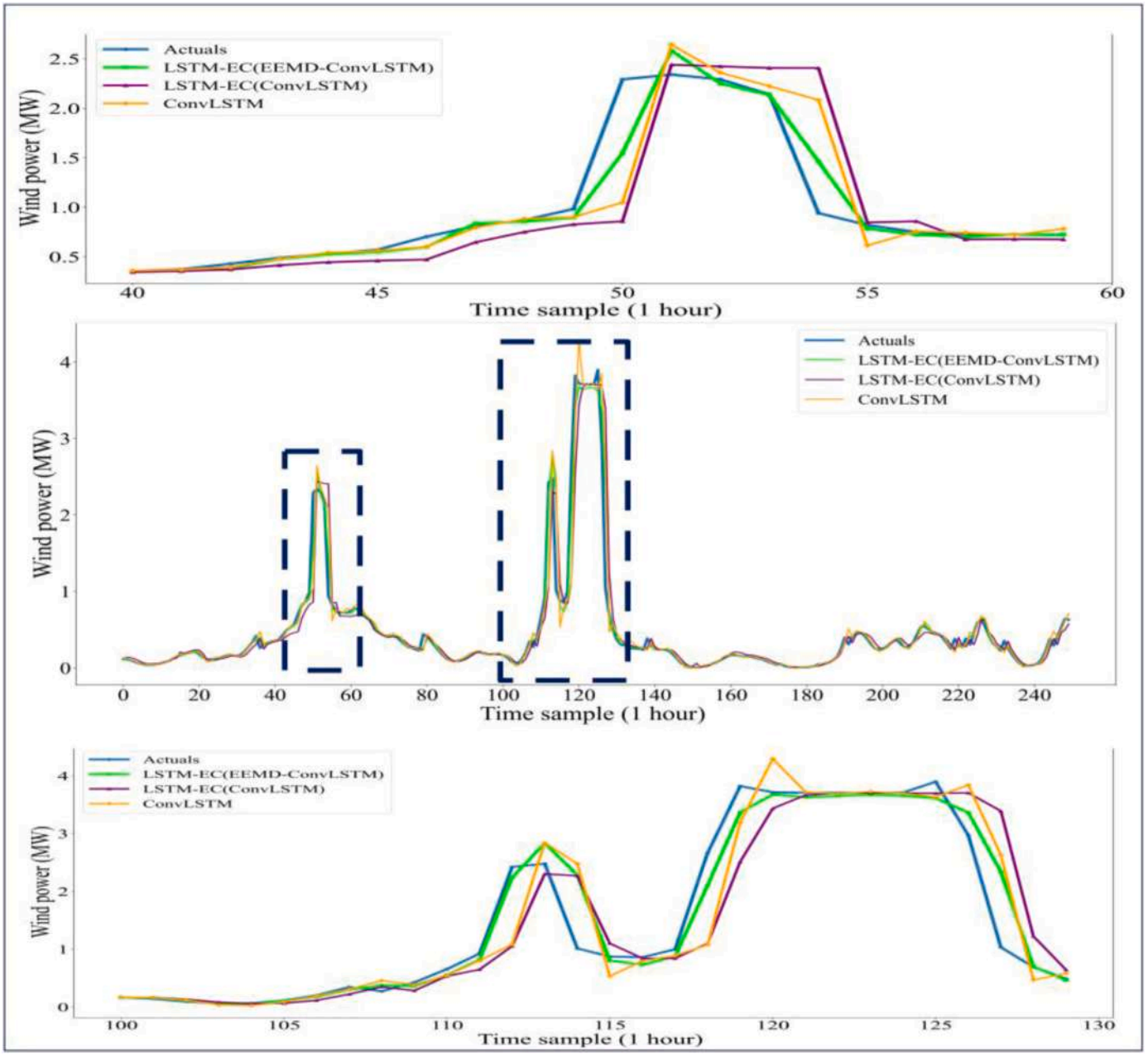

Fig. 13. Proposed model performance wind power forecasting.

and demonstrates reliable forecasting for future time steps in the wind power sequence, with a MAPE of 0.76%. In contrast, the performance of other models deteriorates more sharply in this scenario, particularly the LSTM and ConvLSTM models, which show higher MAE values of 20.899 kW and 19.485 kW, respectively. Traditional models such as ARIMA and SVR face significant challenges, with substantial increases in errors, further emphasizing their limitations in managing longer forecasting horizons. The 3-h forecast plot in Fig. 14 clearly illustrates these results. While the proposed model effectively captures the overall trend of the wind power data, it exhibits more noticeable deviations, particularly near the peaks. This behaviour highlights the inherent challenges of multi-step forecasting, where error propagation and increased uncertainty progressively affect forecast accuracy.

4.4.3. *Four-step forecasting*

The four-step forecasting, as detailed in Table 5 and Fig. 17, represents the most challenging scenario for the models. The LSTM-Error Correction (EEMD-ConvLSTM) model, while maintaining its position as the top-performing model, exhibits a significant increase in error, recording an MAE of 25.505 kW and an RMSE of 56.815 kW. The R^2 value drops to 0.7962, and the MAPE increases to 1.52%, reflecting the increased difficulty of accurately forecasting wind power four steps ahead. The errors in the LSTM-Error Correction (ConvLSTM) and ConvLSTM models continue to rise, with MAE values of 30.249 kW and 40.236 kW, respectively. Traditional models, particularly ARIMA and SVR, perform poorly with MAE values of 97.773 kW and 217.836 kW, respectively. The 4-h ahead forecast plot in Fig. 17 highlights these challenges, showing noticeable gaps between the predicted and actual values. The model frequently overestimates or underestimates wind power, especially at key high and low points. These results assure the limitations of traditional forecasting methods and even some deep learning models in handling long-term power forecasts, where the data's stochastic nature and the accumulation of errors result in significant challenges. On the other hand, the proposed model continues to

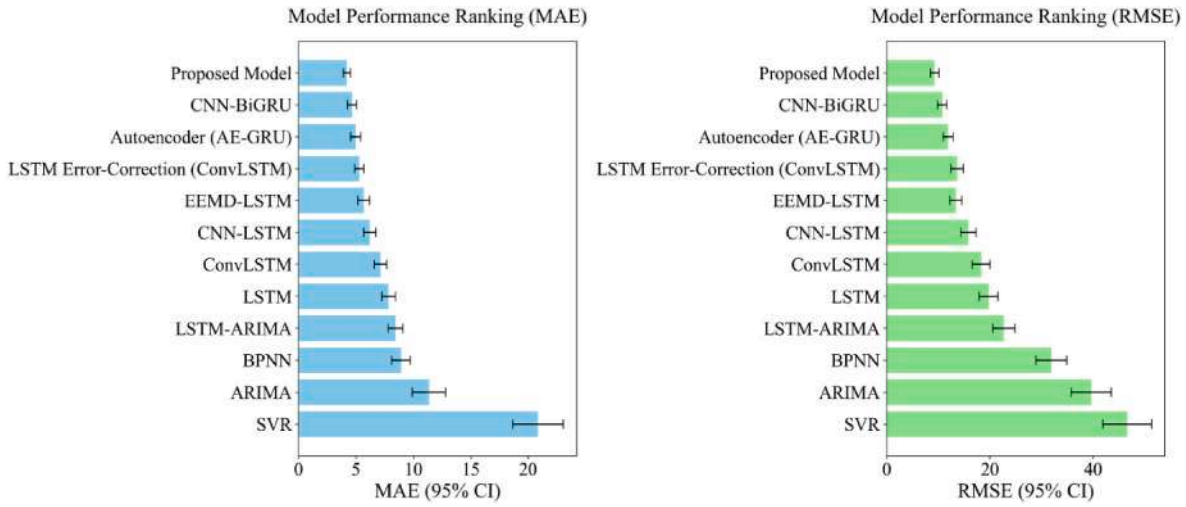

Fig. 14. Model performance comparison MAE and RMSE with 95% confidence intervals.

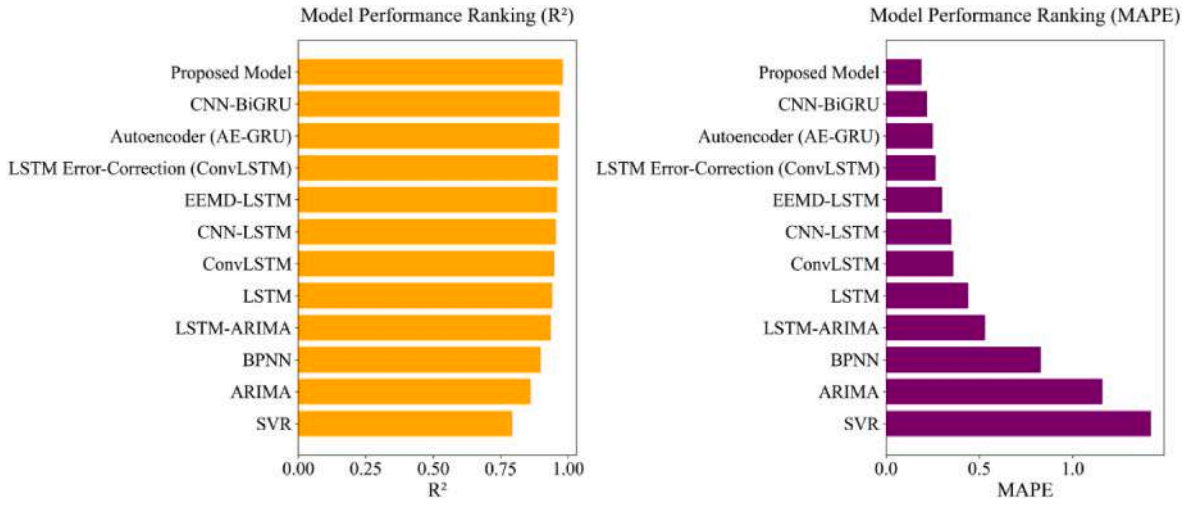

Fig. 15. Model performance comparison: Mape and R^2.

Table 4
Performance Comparison of the proposed model with several hybrid Models in the offshore wind power forecasting (kW).

Model	MAE (95% CI)	RMSE (95% CI)	R^2	MAPE	p-value vs. Proposed Model
LSTM Error-Correction (EEMD-ConvLSTM)	**4.22 ± 0.31**	**9.31 ± 0.80**	**0.9811**	**0.19**	-
CNN-BiGRU	4.51 ± 0.38	10.75 ± 0.90	0.9768	0.22	0.055
Autoencoder (AE-GRU)	4.77 ± 0.42	11.90 ± 0.98	0.9724	0.26	0.044
EEMD-LSTM	5.12 ± 0.50	13.42 ± 1.18	0.9659	0.3	0.035
CNN-LSTM	5.58 ± 0.54	15.84 ± 1.50	0.9553	0.35	0.025
LSTM-ARIMA	6.35 ± 0.60	19.75 ± 1.80	0.9401	0.44	0.01

demonstrate its strength in short-term forecasting, even as the horizon extends. This is achieved through its innovative approach of subtracting wind power forecasting errors across time steps and leveraging a hybrid technique that combines EEMD decomposition with the ConvLSTM model. This powerful combination ensures consistent error correction, enhancing the model's reliability in handling the dynamic and complex challenges that arise with longer forecasting horizons.

5. Conclusion

This study presents an innovative hybrid approach combining EEMD decomposition and ConvLSTM networks for error correction in offshore wind power forecasting. By integrating EEMD and ConvLSTM for error prediction with LSTM, the model achieves enhanced accuracy in wind power forecasting. Using wind power data from a Siemens SWT-3.6-120 offshore turbine, collected at Amrumbank West in a German offshore wind farm between 2015 and 2023, the proposed forecasting model is evaluated for accuracy using error metrics such as MAE, RMSE, MAPE, and R^2. The key conclusions of this research are summarized below.

(1) Using a robust error correction method, the proposed approach effectively corrects and refines original forecasts.
(2) The EEMD decomposition is employed to pre-process the forecasting error signal to capture the complicated and nonlinear patterns within the error signal.

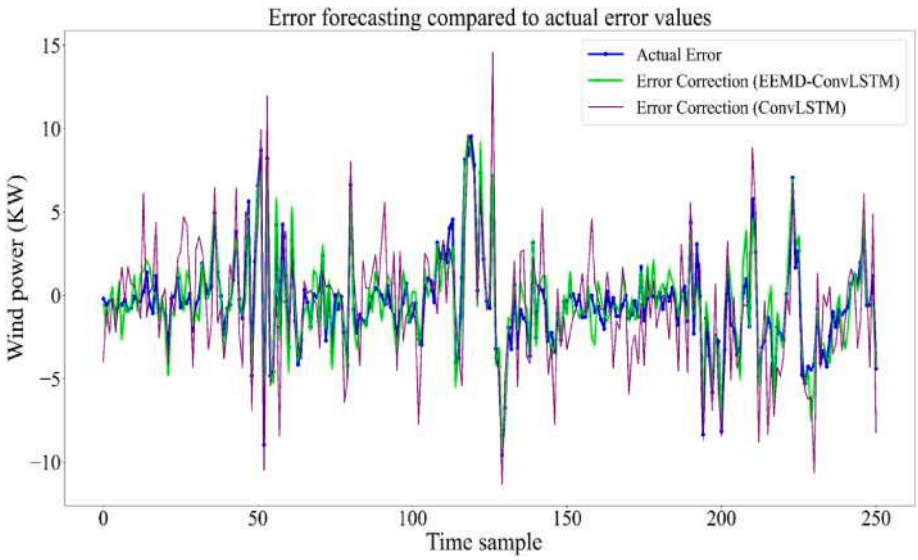

Fig. 16. Forecasted error compared to actual error.

Table 5
Performance error (kW) comparison of the EEMD-ConvLSTM model across various forecasting time steps.

Models	MAE	RMSE	R2	MAPE %
Two steps				
LSTM-Error Correction (EEMD-CONVLSTM)	**7.605**	**13.66**	**0.9396**	**0.39**
LSTM-Error Correction (CONVLSM)	8.801	21.05	0.9157	0.57
CONVLSTM	11.323	36.12	0.8533	0.9
LSTM	12.173	42.92	0.8337	1.14
BPNN	16.635	63.75	0.7764	1.65
ARIMA	24.279	84.53	0.7025	2.27
SVR	50.345	105.38	0.6807	2.98
Three steps				
LSTM-Error correction(EEMD-CONVLSTM)	**12.252**	**26.703**	**0.8936**	**0.76**
LSTM-Error correction(CONVLSM)	14.745	43.648	0.8115	1.31
CONVLSTM	19.485	66.4159	0.7689	1.86
LSTM	20.899	77.146	0.7233	1.91
BPNN	29.973	114.862	0.6737	3.24
ARIMA	45.362	162.45	0.5892	4.59
SVR	97.538	209.023	0.5211	6.54
Four steps				
LSTM-Error correction(EEMD-CONVLSTM)	**25.505**	**56.815**	**0.7962**	**1.52**
LSTM-Error correction(CONVLSM)	30.249	85.95	0.7193	2.06
CONVLSTM	40.236	130.15	0.6981	2.87
LSTM	43.634	162.98	0.6469	3.53
BPNN	67.716	261.31	0.5113	6.79
ARIMA	97.773	344.351	0.4521	9.81
SVR	217.836	437.018	0.3866	14.89

(3) By integrating EEMD and ConvLSTM, the model captures extreme values and noise while extracting spatiotemporal dependencies often missed by standard LSTM models.
(4) The simulation results reveal that the proposed LSTM-Error Correction (EEMD-ConvLSTM), outperforms several relevant deep learning-based forecasting models in terms of error metrics such as RMSE, MAE, MAPE, and R^2. Furthermore, significant improvements across various temporal scales have been achieved.

CRediT authorship contribution statement

Lokmene Melalkia: Writing – original draft, Visualization, Validation, Software, Methodology, Investigation, Formal analysis, Data curation, Conceptualization. **Farid Berrezzek:** Writing – review & editing, Supervision, Methodology, Conceptualization. **Khaled khelil:** Writing – review & editing, Supervision, Resources, Data curation. **Abdelhakim Saim:** Writing – review & editing, Validation, Supervision, Methodology, Formal analysis. **Radouane Nebili:** Writing – review & editing, Validation, Investigation.

Consent to participate

Informed consent was not required for this study.

Consent to publish

All authors have read and agreed to the manuscript being submitted for publication.

6. Limitations and future research

Although the proposed hybrid deep learning model shows promising improvements in offshore wind power forecasting accuracy, several limitations require further examination. First, the integration of EEMD and ConvLSTM layers increases computational complexity, which may hinder real-time applications. Second, the model's sensitivity to noise and outliers in the data could affect its reliability. Third, a more comprehensive exploration of the hyperparameter space could further improve accuracy and robustness.

Future research should focus on.

1. Develop robust data preprocessing techniques to handle noise, outliers, and missing data.
2. Exploring alternative decomposition methods, to reduce computational complexity and improve noise resilience, thereby minimizing outlier data values even further.
3. Investigating transfer learning approaches to enhance model generalizability across diverse wind farms.
4. Designing lightweight and computationally efficient architectures for real-time applications.

Addressing these limitations and pursuing these directions will advance the development of more accurate, reliable, and practical wind power forecasting models.

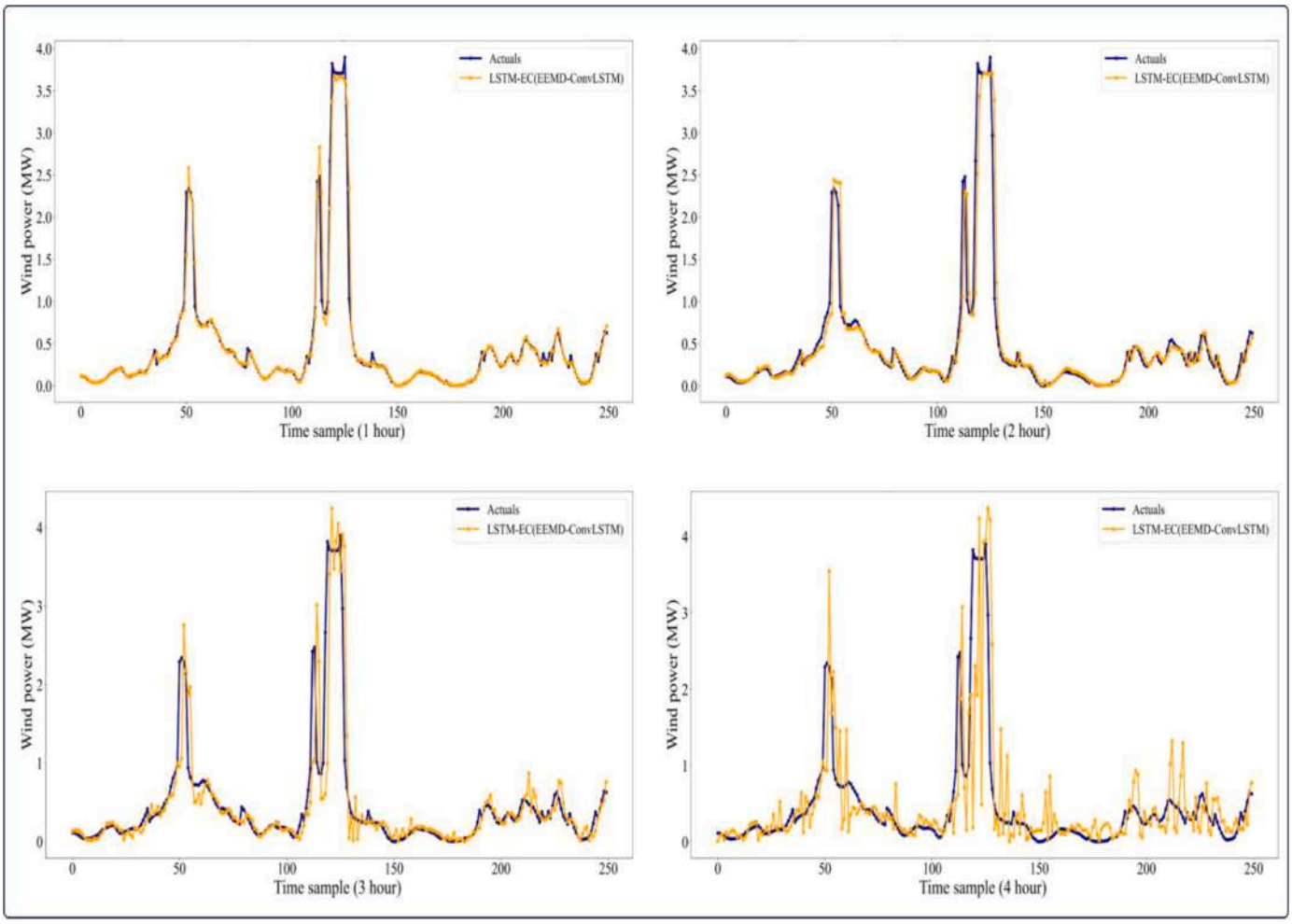

Fig. 17. The proposed LSTM-Error Correction (EEMD-ConvLSTM) forecasting model over different time horizons.

Ethical approval

This research did not require ethical approval.

Availability of data and materials

Data will be made available on reasonable request.

Funding

No funding has been received.

Declaration of competing interest

The authors declare that they have no known competing financial interests or personal relationships that could have appeared to influence the work reported in this paper.

Acknowledgement

This work is supported by the Directorate General of Scientific Research and Technological Development (DGRSDT), Algeria.

References

Berrezzek, F., Khelil, K., Bouadjila, T., 2019. Efficient wind speed forecasting using discrete wavelet transform and artificial neural networks. Rev d'Intelligence Artif 33, 447–452. https://doi.org/10.18280/ria.330607.

Bouadjila, T., Khelil, K., Rahem, D., Berrezzek, F., 2024. Hourly solar irradiance forecasting using long short term memory and convolutional neural networks. Smart Grids Sustain Energy 9. https://doi.org/10.1007/s40866-024-00224-2.

Cai, H., Wu, Z., Huang, C., Huang, D., 2019. Wind power forecasting based on ensemble empirical mode decomposition with generalized regression neural network based on cross-validated method. J Electr Eng Technol 14, 1823–1829. https://doi.org/10.1007/s42835-019-00186-x.

Erdem, E., Shi, J., She, Y., 2014. Comparison of two ARMA-GARCH approaches for forecasting the mean and volatility of wind speed. Springer Proc. Phys. 155, 65–73. https://doi.org/10.1007/978-3-319-05521-3_9.

Garg, S., Krishnamurthi, R., 2023. A CNN encoder decoder LSTM model for sustainable wind power predictive analytics. Sustain Comput Informatics Syst 38, 100869. https://doi.org/10.1016/j.suscom.2023.100869.

Greenland, S., Senn, S.J., Rothman, K.J., et al., 2016. Statistical tests, P values, confidence intervals, and power: a guide to misinterpretations. Eur. J. Epidemiol. 31, 337–350. https://doi.org/10.1007/s10654-016-0149-3.

Guo, J., Lin, P., Zhang, L., et al., 2023. Dynamic adaptive encoder-decoder deep learning networks for multivariate time series forecasting of building energy consumption. Appl. Energy 350, 121803. https://doi.org/10.1016/j.apenergy.2023.121803.

Guo, L., Xu, C., Yu, T., et al., 2024. Ultra-short-term wind power forecasting based on long short-term memory network with modified honey badger algorithm. Energy Rep. 12, 3548–3565. https://doi.org/10.1016/j.egyr.2024.09.021.

Hauber, A.B., González, J.M., Groothuis-Oudshoorn, C.G.M., et al., 2016. Statistical methods for the analysis of discrete choice experiments: a report of the ispor conjoint analysis good research practices task force. Value Health 19, 300–315. https://doi.org/10.1016/j.jval.2016.04.004.

Hou, G., Wang, J., Fan, Y., 2024. Multistep short-term wind power forecasting model based on secondary decomposition, the kernel principal component analysis, an enhanced arithmetic optimization algorithm, and error correction. Energy 286, 129640. https://doi.org/10.1016/j.energy.2023.129640.

Jiang, T., Liu, Y., 2023. A short-term wind power prediction approach based on ensemble empirical mode decomposition and improved long short-term memory. Comput. Electr. Eng. 110, 108830. https://doi.org/10.1016/j.compeleceng.2023.108830.

Khelil, K., Berrezzek, F., Bouadjila, T., 2021. GA-based design of optimal discrete wavelet filters for efficient wind speed forecasting. Neural Comput. Appl. 33, 4373–4386. https://doi.org/10.1007/s00521-020-05251-5.

Mo, Y., Wang, H., Yang, C., et al., 2024. Jou lP. Energy, 133514. https://doi.org/10.1016/j.energy.2024.133514.

Moharm, K., Eltahan, M., Elsaadany, E., 2020. Wind speed forecast using LSTM and Bi-LSTM algorithms over gabal el-zayt wind farm. Proc - 2020 Int Conf Smart Grids Energy Syst SGES 2020, 922–927. https://doi.org/10.1109/SGES51519.2020.00169.

Shahid, F., Mehmood, A., Khan, R., et al., 2023. 1D Convolutional LSTM-based wind power prediction integrated with PkNN data imputation technique. J King Saud Univ - Comput Inf Sci, 101816. https://doi.org/10.1016/j.jksuci.2023.101816.

Shukur, O.B., Lee, M.H., 2015. Daily wind speed forecasting through hybrid KF-ANN model based on ARIMA. Renew. Energy 76, 637–647. https://doi.org/10.1016/j.renene.2014.11.084.

Sun, W., Wang, X., 2023. Improved chimpanzee algorithm based on CEEMDAN combination to optimize ELM short-term wind speed prediction. Environ. Sci. Pollut. Res. 30, 35115–35126. https://doi.org/10.1007/s11356-022-24586-1.

Wan, A., Chang, Q., Al-Bukhaiti, K., He, J., 2023. Short-term power load forecasting for combined heat and power using CNN-LSTM enhanced by attention mechanism. Energy 282, 128274. https://doi.org/10.1016/j.energy.2023.128274.

Wang, J., Qian, Y., Zhang, L., et al., 2024. A novel wind power forecasting system integrating time series refining, nonlinear multi-objective optimized deep learning and linear error correction. Energy Convers. Manag. 299, 117818. https://doi.org/10.1016/j.enconman.2023.117818.

Wilkerson, S., Wilkerson, S.D., 2008. Application of the paired t-test. Undergrad Res Journal Sch Note 5, 4–5.

Xin, Z., Liu, X., Zhang, H., et al., 2024. An enhanced feature extraction based long short-term memory neural network for wind power forecasting via considering the missing data reconstruction. Energy Rep. 11, 97–114. https://doi.org/10.1016/j.egyr.2023.11.040.

Yang, W., Zhang, H., Lim, J.B., et al., 2024. A new chiller fault diagnosis method under the imbalanced data environment via combining an improved generative adversarial network with an enhanced deep extreme learning machine. Eng. Appl. Artif. Intell. 137. https://doi.org/10.1016/j.engappai.2024.109218.

Yu, H., Hutson, A.D., 2024. A robust Spearman correlation coefficient permutation test. Commun. Stat. Theor. Methods 53, 2141–2153. https://doi.org/10.1080/03610926.2022.2121144.

Yu, C., Li, Y., Bao, Y., et al., 2018. A novel framework for wind speed prediction based on recurrent neural networks and support vector machine. Energy Convers. Manag. 178, 137–145. https://doi.org/10.1016/j.enconman.2018.10.008.

Zhang, W., Lin, Z., Liu, X., 2022a. Short-term offshore wind power forecasting - a hybrid model based on discrete wavelet transform (DWT), seasonal autoregressive integrated moving average (SARIMA), and deep-learning-based long short-term memory (LSTM). Renew. Energy 185, 611–628. https://doi.org/10.1016/j.renene.2021.12.100.

Zhang, H., Li, C., Wei, Q., Zhang, Y., 2022b. Fault detection and diagnosis of the air handling unit via combining the feature sparse representation based dynamic SFA and the LSTM network. Energy Build. 269, 112241. https://doi.org/10.1016/j.enbuild.2022.112241.

Zhao, Z., Yun, S., Jia, L., et al., 2023. Hybrid VMD-CNN-GRU-based model for short-term forecasting of wind power considering spatio-temporal features. Eng. Appl. Artif. Intell. 121, 105982. https://doi.org/10.1016/j.engappai.2023.105982.

Zhao, Y., Zhang, W., Liu, X., 2024. Grid search with a weighted error function: hyper-parameter optimization for financial time series forecasting. Appl. Soft Comput. 154, 111362. https://doi.org/10.1016/j.asoc.2024.111362.

Zheng, S., Chen, S., Chen, T., et al., 2024. Deep learning-based SNR estimation. IEEE Open J Commun Soc 5, 4778–4796. https://doi.org/10.1109/OJCOMS.2024.3436640.